Biochimica et Biophysica Acta 1797 (2010) 1398–1409

Contents lists available at ScienceDirect

Biochimica et Biophysica Acta

journal homepage: www.elsevier.com/locate/bbabio

Specific motifs of the V-ATPase a2-subunit isoform interact with catalytic and regulatory domains of ARNO

Maria Merkulova [a], Anastasia Bakulina [b], Youg Raj Thaker [c], Gerhard Grüber [c,d], Vladimir Marshansky [a,*]

[a] Center for Systems Biology, Program in Membrane Biology and Division of Nephrology, Department of Medicine, Massachusetts General Hospital and Harvard Medical School, Boston, MA, 02114, USA

[b] State Research Center of Virology and Biotechnology "VECTOR", Koltsovo, Novosibirsk Region, 630559, Russia

[c] Nanyang Technological University, Division of Structural and Computational Biology, School of Biological Sciences, 60 Nanyang Drive, Singapore 637551, Republic of Singapore

[d] Bioinformatics Institute (A*STAR), 30 Biopolis Street, #07-01 Matrix, Singapore 138671, Republic of Singapore

ARTICLE INFO

Article history:
Received 27 August 2009
Received in revised form 11 January 2010
Accepted 8 February 2010
Available online 11 February 2010

Keywords:
V-type ATPase
Arf-GEF ARNO
Sec7-domain
PB-domain
BIAcore
NMR
Peptide structure
Phosphorylation

ABSTRACT

We have previously shown that the V-ATPase a2-subunit isoform interacts specifically, and in an intra-endosomal acidification-dependent manner, with the Arf-GEF ARNO. In the present study, we examined the molecular mechanism of this interaction using synthetic peptides and purified recombinant proteins in protein-association assays. In these experiments, we revealed the involvement of multiple sites on the N-terminus of the V-ATPase a2-subunit (a2N) in the association with ARNO. While six a2N-derived peptides interact with wild-type ARNO, only two of them (named a2N-01 and a2N-03) bind to its catalytic Sec7-domain. However, of these, only the a2N-01 peptide (MGSLFRSESMCLAQLFL) showed specificity towards the Sec7-domain compared to other domains of the ARNO protein. Surface plasmon resonance kinetic analysis revealed a very strong binding affinity between this a2N-01 peptide and the Sec7-domain of ARNO, with dissociation constant $K_D = 3.44 \times 10^{-7}$ M, similar to the $K_D = 3.13 \times 10^{-7}$ M binding affinity between wild-type a2N and the full-length ARNO protein. In further pull-down experiments, we also revealed the involvement of multiple sites on ARNO itself in the association with a2N. However, while its catalytic Sec7-domain has the strongest interaction, the PH-, and PB-domains show much weaker binding to a2N. Interestingly, an interaction of the a2N to a peptide corresponding to ARNO's PB-domain was abolished by phosphorylation of ARNO residue Ser_{392}. The 3D-structures of the non-phosphorylated and phosphorylated peptides were resolved by NMR spectroscopy, and we have identified rearrangements resulting from Ser_{392} phosphorylation. Homology modeling suggests that these alterations may modulate the access of the a2N to its interaction pocket on ARNO that is formed by the Sec7 and PB-domains. Overall, our data indicate that the interaction between the a2-subunit of V-ATPase and ARNO is a complex process involving various binding sites on both proteins. Importantly, the binding affinity between the a2-subunit and ARNO is in the same range as those previously reported for the intramolecular association of subunits within V-ATPase complex itself, indicating an important cell biological role for the interaction between the V-ATPase and small GTPase regulatory proteins.

1. Introduction

Vesicular trafficking within both endocytotic and exocytotic pathways is an essential cellular process for the function of eukaryotic cells. In particular, endocytosis is widely used by mammalian cells to internalize an enormous variety of macromolecules such as proteins, nutrients, toxins, DNA, RNA as well as microorganisms including viruses and bacteria. The proper function of both pathways requires the acidification of the lumen of their constituent organelles, which is driven by the vacuolar-type H^+-ATPase (V-ATPase). While the role of the V-ATPase in acidifying intracellular compartments and extracellular spaces has been long established, we recently uncovered a novel function of the V-ATPase as an endosomal pH-sensing receptor that interacts with and recruits Arf-family small GTPases and their

Abbreviations: V-ATPase, vacuolar-type H^+-ATPase; a2N, N-terminal cytosolic tail of V-ATPase a2-subunit isoform; ARNO, ADP-ribosylation factor nucleotide site opener; Arf6, ADP-ribosylation factor 6; GEF, GDP/GTP-exchange factor; GAP, GTPase-activating protein; GST, glutathione-S-transferase; SPR, surface plasmon resonance; NMR, nuclear magnetic resonance; NOESY, nuclear Overhauser effect spectroscopy; TOCSY, total correlation spectroscopy; CC-domain, coiled-coil domain; PH-domain, pleckstrin homology domain; PB-domain, polybasic domain; PKC, protein kinase C; Ser_{392}, serine392

* Corresponding author. Center for Systems Biology, Program in Membrane Biology and Division of Nephrology, Simches Research Center, Massachusetts General Hospital, 185 Cambridge Street, CPZN, Suite #8212, Boston, MA, 02114, USA. Tel.: +1 617 724 9815; fax: +1 617 643 3182.

E-mail address: Vladimir_Marshansky@hms.harvard.edu (V. Marshansky).

0005-2728/$ – see front matter © 2010 Elsevier B.V. All rights reserved.
doi:10.1016/j.bbabio.2010.02.009

regulatory proteins to endosomal membranes [1,2]. It was demonstrated that these cell biological events take place on early endosomes and are crucial for regulation of the endosomal/lysosomal protein degradative pathway. Based on these findings, we hypothesized that cross-talk between the V-ATPase and Arf small GTPases may extend to acidic organelles in general.

The V-ATPase is a multimeric complex that functions as a proton pumping nano-motor [3]. Its cytoplasmic V_1-sector is involved in ATP hydrolysis and is composed of eight different subunits arranged in the following stoichiometry (A_3:B_3:C_1:D_1:E_3:F_1:G_3:H_1) [4–6]. The transmembrane V_O-sector is composed of six different subunits (a_1:c_4:c'_1:c''_1:d_1:e_1) and is responsible for proton translocation across the lipid bilayer. V-ATPase structure as well as its cell biological functions and biochemical regulation have been previously reviewed in detail [7–12]. The transmembrane a-subunit of the V-ATPase is a ~100 kDa protein consisting of two dissimilar parts: i) an N-terminal hydrophilic cytosolic tail and ii) a C-terminal hydrophobic part with eight putative transmembrane helices [2,13]. Four a-subunit isoforms (a1, a2, a3 and a4) are found in mammals [9,14–17]. These subunits are responsible for proper assembly of the V-ATPase and for its differential targeting to a variety of intracellular organelles and to the plasma membrane of some specialized cells [3]. Cross-linking, two-hybrid screening and co-immunoprecipitation experiments showed that the a-subunit isoforms interact with A-, E-, H-, C-, and G-subunits of the V_1 sector [18–22]. Moreover, increasing experimental evidence indicates that the cytosolic tails of a-subunit isoforms also interact with an enzyme of the glycolytic pathway, aldolase B [23–26], which is involved in glucose-dependent reversible assembly/disassembly of the V_O and V_1 sectors, an important regulatory mechanism of V-ATPase function. Furthermore, another enzyme of the glycolytic pathway, phosphofrucktokinase-1, directly interacts with the a4-isoform and is involved in regulation of the function of human V-ATPase [27,28].

ADP-ribosylation factors (Arf) belong to the Ras-superfamily of small GTPases. These proteins function as molecular switches and regulate a variety of cell biological events within both endocytotic and exocytotic trafficking pathways [29–31]. The Arf-family consists of six members that are categorized into three classes: class I (Arf1, Arf2, Arf3), class II (Arf4, Arf5) and class III, which is represented by Arf6. The activation of Arfs ("on"-state in the GTP-bound form) is driven by guanine nucleotide exchange factors (GEFs), while their deactivation ("off"-state in the GDP-bound form) is catalyzed by GTPase-activating proteins (GAPs). Recently, it has been shown that the cytohesin-family of Arf-GEFs, like Arfs themselves, cycle between inactive and active conformations, resulting in even more tight regulation of Arf activation [32]. Since GDP/GTP-exchange is coupled to high-affinity membrane binding of Arfs, Arf-GEFs are also responsible for recruiting Arfs to specific membrane domains and are, thus, capable of regulating Arf activity in a spatial manner. Although several Arf-specific GEFs and GAPs were shown to interact with more than one Arf-family member *in vitro*, more recent data indicate that each Arf-family member is regulated by distinct GEFs and GAPs *in vivo*. All known Arf-GEFs contain a highly conserved Sec7 catalytic domain, which is responsible for GEF activity and is related to the prototype yeast protein Sec7p. To date fifteen Sec7 family members have been identified in the human genome [33]. ARNO (also known as, cytohesin-2) is a member of the cytohesin subfamily of Arf-GEFs, which includes another three members: cytohesin-1, cytohesin-3 (also called ARNO3 or GRP1) and cytohesin-4 [33]. Human cytohesins exhibit at least 80% similarity in a pairwise comparison of their amino acid sequences and share a common domain organization. Their structure is divided into the following four regions: i) an N-terminal coiled-coil (CC) domain; ii) a central Sec7-domain; iii) a pleckstrin homology (PH) domain; and iv) a C-terminal polybasic (PB) domain. In ARNO, the PB-domain is phosphorylated at serine392 (Ser_{392}) by protein kinase C (PKC), which regulates Arf-GEF activity [34]. Recently, a high-resolution crystal structure of GRP1 (lacking the CC-domain) revealed the regulatory importance of a structure connecting the Sec7 and PH-domains (Sec7-PH-linker) which, together with the PB-domain, is involved in cytohesin autoinhibition [32].

Previously we identified the V-ATPase as an endosomal pH-sensor that scaffolds the cytosolic Arf-GEF ARNO and Arf6 [1,2]. In particular, we demonstrated that the transmembrane a2-subunit isoform of the V-ATPase directly interacts with ARNO in an acidification-dependent manner. This biochemical event is essential for vesicular trafficking between early and late endosomes of the endosomal/lysosomal protein degradative pathway. However, the molecular details of the a2-subunit/ARNO interaction and the cell biological significance of this rendezvous in regulating the V-ATPase/ARNO/Arf6 complex remain unknown. In this study we address these questions and have uncovered an elaborate, multisite interaction between the V-ATPase a2-subunit isoform and ARNO, which could be involved in the regulation of enzymatic activities within this complex.

2. Materials and methods

2.1. Reagents and antibodies

If not otherwise specified, all reagents were from Sigma (St. Louis, MO). NU-PAGE gels and buffers were from Invitrogen (Carlsbad, CA). Criterion gels were from Bio-Rad (Hercules, CA). Protease inhibitor tablets Complete EDTA-free were from Roche (Indianapolis, IN). Western Lightning™ Plus chemiluminescence reagent was from PerkinElmer (Boston, MA). Streptavidin, immobilized on Agarose CL-4B was from Fluka (St. Louis, MO). TALON metal affinity resin was from Clontech (Mountain View, CA). Glutathione Sepharose 4B, Superdex™ 200 HR 10/30 pre-packed column and HRP-conjugated sheep anti-mouse and goat anti-rabbit IgGs were from GE Healthcare (Pitscataway, NJ). Monoclonal anti-GST antibodies (Clone B-14) were purchased from Santa Cruz Biotechnology (Santa Cruz, CA). Production and characterization of specific rabbit polyclonal antibodies against the a2 subunit isoform of the V-ATPase was previously described [1].

2.2. Synthetic peptides

Peptides were synthesized, purified by HPLC and analyzed by mass spectrometry in the MGH Peptide/Protein Core Facility. All a2N-derived peptides were synthesized with a biotin-tag on the N-terminus for immobilization on streptavidin-agarose beads and with an additional C-terminal cysteine residue for immobilization on beads using sulfhydryl-specific crosslinkers. A peptide corresponding to the PB-domain of ARNO was synthesized containing either a non-phosphorylated or a phosphorylated Ser_{392} residue. Peptide stock solutions were prepared in DMSO at 5 mM concentration and stored at −20 °C.

2.3. DNA constructs, protein expression and purification

Constructs corresponding to amino acid residues 1–133 (a2N-N) and 134–393 (a2N-C) of the mouse V-ATPase a2-isoform were amplified using Expand High Fidelity PCR System and subcloned into a pIVEX2.4d vector (Roche, Indianapolis, IN) using NcoI/SmaI restriction sites. The resulting constructs contain a modified N-terminal 6XHis-tag (MSGSHHHHHHSSGIEGRGRLIKMT). Both constructs were *in vitro* translated using the RTS100 kit (Roche, Indianapolis, IN) and used in pull-down experiments. A construct corresponding to amino acid residues 1–402 of mouse V-ATPase a2-isoform (a2N) was amplified as above and subcloned into NdeI/NotI restriction sites of pET28b vector (Novagen, Gibbstown, NJ) in frame with a thrombin cleavable N-terminal 6XHis-tag. Recombinant a2N protein was expressed in *E. coli* BL21(DE3) cells and purified from inclusion bodies under denaturing conditions (in the presence of 6 M Guanidine–HCL) on Talon beads (Clontech) and refolded into 1 M NDSB-256, 100 mM CHES–NaOH, pH

9.0, and 1 mM DTT. Conditions for refolding were found by screening with iFOLD™ Protein Refolding System 2 (Novagen, Gibbstown, NJ). After refolding, a2N protein was dialysed into 100 mM CHES–NaOH, pH 9.0, and 1 mM DTT immediately prior to immobilization on BIAcore chip.

Cytohesin-2 or ARNO is a highly conserved protein with 99.25% identity between human and mouse species. There are only three similar substitutions between human and mouse amino acids N86H, A124S and E229D in ARNO sequences. Thus, in our experiments we used human ARNO, since the crystal structure of its Sec7-domain in complex with Arf1 has been previously solved and was used in our modeling studies. The following constructs corresponding to wild-type human ARNO (triglycine variant) and its domains were generated: i) 1–400aa, full-length ARNO(wt); ii) 1–60aa, coiled-coil (CC) domain; iii) 61–252aa, Sec7-domain; iv) 253-378aa, plekstrin-homology (PH) domain; and v) 379–400aa, polybasic (PB) domain. All domains of ARNO were amplified with simultaneous incorporation of a 6XHis tag using Expand High Fidelity PCR System and subcloned into pGEX6P-1 vector (GE Healthcare, Pitscataway, NJ) using EcoRI/NotI restriction sites. The resulting constructs contain an N-terminal GST-tag and a C-terminal 6XHis tag. All five recombinant proteins were expressed in *E. coli* BL21(DE3) cells (Stratagene) and were purified by sequential chromatography on TALON beads (Clontech) and glutathione Sepharose 4B beads (GE Healthcare) according to the manufacturer's instructions. Alternatively, GST-tagged ARNO(wt) was purified by sequential chromatography on glutathione Sepharose 4B beads (GE Healthcare) and Superdex™ 200 HR 10/30 pre-packed column (GE Healthcare) using the "AKTA Purifier" system (GE Healthcare) according to the manufacturer's instructions. For BIAcore experiments, the GST-tag was cleaved from the Sec7-domain by PreScission Protease™ (GE Healthcare) according to the manufacturer's instructions.

2.4. Biotinylated peptide pull-down assay

All a2N-derived peptides were immobilized by an N-terminal biotin-tag, which ensures the same efficiency and equivalent binding to streptavidin-agarose beads. Simultaneous pull-down experiments with immobilized peptides were performed using highly purified recombinant GST-ARNO(wt) or GST-Sec7-6His as described below. First, equal amounts (7 nmol) of the corresponding 22 synthetic peptides were immobilized on 25 µl of 50% streptavidin-agarose CL-4B (Fluka) slurry by mixing them overnight at 4 °C in 500 µl of binding buffer (10 mM HEPES pH 7.5, 1 mM EDTA, 1 mM DTT, 100 mM NaCl, 10% glycerol, 0.1% NP-40). To remove unbound peptides, beads were collected by centrifugation and washed in 500 µl ice-cold binding buffer. Next, equal amounts (20 pmol) of highly purified recombinant GST-ARNO(wt) or GST-Sec7-6His were added to the beads containing immobilized peptides and incubated for 2 h at 4 °C in 500 µl of binding buffer. After washing beads four times in ice-cold binding buffer, the interacting GST-ARNO/a2N-derived peptide complexes were eluted by boiling in SDS-PAGE sample buffer for 10 min at 95 °C, resolved by SDS-PAGE and analyzed by Western blotting using monoclonal anti-GST antibody. In pull-down experiments with ARNO-derived peptides, equal amounts (7 nmol) of biotin-tagged synthetic peptides were also immobilized on streptavidin-agarose beads followed by incubation with 10 µl of *in vitro* translated 6His-a2N(wt) recombinant protein. Pull-down experiments and SDS-PAGE analysis were performed as described above and interacting 6His-a2N/ARNO-derived peptide complexes were analyzed by Western blotting using polyclonal anti-a2N antibody. All experiments were repeated at least three times with similar results.

2.5. GST fusion protein pull-down assay

In this assay, the direct interaction of recombinant proteins was studied. The purified recombinant GST-ARNO(wt) and GST-tagged ARNO domain constructs (100 pmol) were incubated with 10 µl of *in vitro* translated 6His-a2N recombinant protein at 4 °C for 2 h in 500 µl of binding buffer (10 mM HEPES, 1 mM EDTA, 1 mM DTT, 100 mM NaCl, 10% glycerol, 0.1% NP-40) with gentle rotation. Then the interacting recombinant proteins were immobilized on glutathione beads by incubation with 50 µl of 50% glutathione Sepharose 4B slurry for 2 h at 4 °C. The beads were collected by centrifugation and washed 5 times with 500 µl ice-cold binding buffer. Interacting proteins were eluted by boiling in SDS-PAGE sample buffer for 10 min at 95 °C, resolved by SDS-PAGE and analyzed by Western blotting using polyclonal anti-a2N antibodies. Alternatively, pull-down experiments with GST-ARNO(wt) and GST-only as control were performed using *in vitro* translated and methionine-^{35}S metabolically labeled recombinant proteins a2N-N-[^{35}S] and a2N-C-[^{35}S], corresponding, respectively, to N-terminal ($a2N_{1-133}$) and C-terminal ($a2N_{134-393}$) parts of a2N. Pull-down experiments and analysis by autoradiography were performed as previously described [1]. All experiments were repeated at least three times.

2.6. Real-time binding and kinetic analysis by surface plasmon resonance (SPR)

SPR binding assays were performed at 25 °C on a BIAcore™ T100 instrument (GE Healthcare). All reagents, including buffers, sensor chips and the amine coupling kit, were obtained from GE Healthcare. For kinetic analysis of the binding of ARNO(wt) with a2N(wt), purified 6His-a2N (5 µg/ml) in 10 mM sodium acetate (pH 4.0) was immobilized at 80 response units (RU) on a CM4 sensor chip using an amine coupling kit according to the manufacturer's instructions. The same kit was used to perform blank immobilization to create a reference surface on the same chip. Samples of purified GST-ARNO (wt) at concentrations ranging from 0.25 to 4 µM were injected for 6 min over active and reference surfaces at a flow rate of 30 µl/min in NBS-EP, 1 mM DTT running buffer (10 mM Hepes, pH 7.4, 150 mM NaCl, 3 mM EDTA, 0.05% Surfactant P20, 1 mM DTT). For kinetic analysis of the binding of the ARNO Sec7-domain with a2N-01 peptide, neutravidin (10 µg/ml) in 10 mM sodium acetate (pH 5.0) was immobilized at about 1200 RU on two surfaces of a CM4 sensor chip using an amine coupling kit. Following that, biotinylated a2N-01 peptide (50 RU) and amine-PEG_3-biotin (25 RU) were irreversibly captured by neutravidin to create active and a reference surfaces, respectively. Purified Sec7-6His recombinant protein was injected for 3.5 min over active and reference surfaces at concentrations ranging from 0.05 to 1 µM and a flow rate of 100 µl/min in NBS-EP, 1 mM DTT running buffer. Dissociation of the complexes was monitored for 10 min, and then the regeneration of the sensor surfaces was performed using 0.05% SDS with 1-min injection in the running buffer at a 20 µl/min flow rate. BIAcore™ T100 Evaluation software was used to calculate the association and dissociation rate constants (k_{on} and k_{off}) with a 1:1 fitting model. The dissociation constant (K_D) was determined from the k_{on}/k_{off} values. To estimate affinity of interaction the corresponding free energy of binding $\Delta G_{bind} = RT\ln K_D$ was calculated as previously described [35].

2.7. NMR data collection, processing and peptide structure calculation

The non-phosphorylated ($ARNO_{375-400}$) and phosphorylated ($ARNO_{375-400}^{P}$) peptides (2 mM final concentration of each peptide) of ARNO were prepared by dissolving an appropriate amount in 50 mM phosphate buffer, pH 6.8. The one dimensional (1D) and two dimensional (2D) ^{1}H NMR spectra including total correlation spectroscopy (TOCSY) and nuclear Overhauser enhancement spectroscopy (NOESY) were obtained at a temperature of 288 K on an Avance Bruker NMR spectrometer at 700 MHz proton frequency. TOCSY and NOESY spectra of the peptide were recorded with mixing times of 80 and 300 ms, respectively. All the NMR data were processed

using the Bruker Avance spectrometer built-in software Topspin. Peak-picking and data analysis of the Fourier-transformed spectra were performed with the SPARKY program [36]. Assignments were carried out according to classical procedures including spin-system identification and sequential assignment [37]. The three-dimensional structure of the peptides $ARNO_{375-400}$ and $ARNO_{375-400}{}^{P}$ were calculated based on both distance and angle restraints by using the CYANA 2.1 program package [38]. Dihedral angle restraints were calculated from chemical shifts using torsion angle likelihood obtained from shift and sequence similarity (TALOS) [37]. In total twenty $ARNO_{375-400}$ and twenty $ARNO_{375-400}{}^{P}$ structures were calculated.

2.8. Bioinformatics analysis and ARNO homology modeling

The prediction of coiled-coil regions and the secondary structure of a2N, used in the design and synthesis of peptides was carried out by direct submission of the a2N amino acid sequence to the following websites (http://www.ch.embnet.org/software/COILSform.html) [39] and (http://bioinf.cs.ucl.ac.uk/psipred/psiform.html) [40,41]. The spatial structure of human ARNO was performed by homology modeling using Modeller9v2 and Gromacs software [42].

3. Results

3.1. Mapping the binding sites on the N-terminal cytosolic tail of the V-ATPase a2-isoform (a2N) that are involved in interaction with ARNO

In order to map the a2N motifs that interact with ARNO, an a2N-derived peptide pull-down approach was applied. Since the three-dimensional structure of V-ATPase a-subunit isoforms is currently unknown, the rational design of a2N-derived peptides was performed using a prediction of the secondary structure for mouse a2N using the PSIPRED server (http://bioinf.cs.ucl.ac.uk/psipred/psiform.html) [40,41]. Moreover, the presence of coiled-coil domains was also predicted on a2N using COILS software (http://www.ch.embnet.org/software/COILS_form.html) [39]. According to this program, the mouse V-ATPase a2-isoform CC-domain spans from L92 to Y128. Using these two *in silico* prediction programs for guidance, 22 peptides covering the 1–402 amino acids of a2N were designed (Fig. 1a) and synthesized (Fig. 1b). Recently, the involvement of CC-motifs in an interaction with syntaxin was demonstrated for the a1-isoform of V-ATPase from *Drosophila melanogaster* [43]. Therefore, in order to test its possible involvement in interaction with ARNO the longest peptide a2N-06 ($a2N_{92-127}$) corresponding to the predicted CC-domain of a2N was synthesized.

a

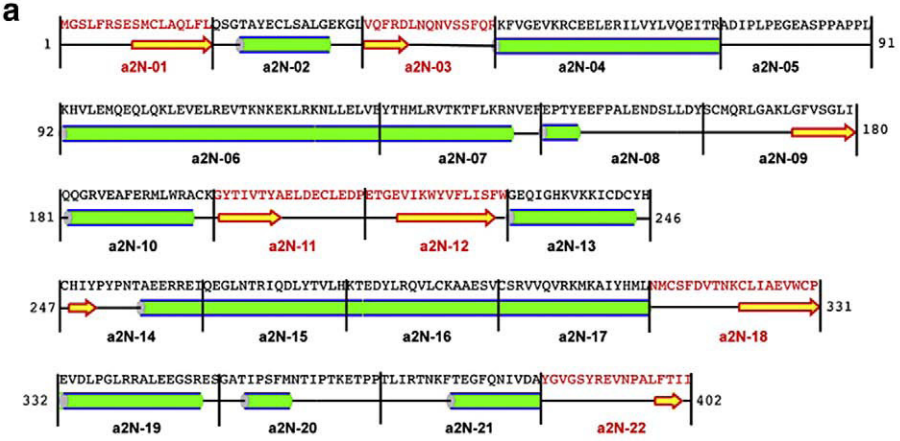

b

Peptide Name	AA of a2N	#AA	AA Sequence of the synthesized peptides
a2N-01	1-17	17	Bio-MGSLFRSESMCLAQLFL-Cys
a2N-02	18-34	17	Bio-QSGTAYECLSALGEKGL-Cys
a2N-03	35-49	15	Bio-VQFRDLNQNVSSFQR-Cys
a2N-04	50-74	25	Bio-KFVGEVKRCEELERILVYLVQEITR-Cys
a2N-05	75-91	17	Bio-ADIPLPEGEASPPAPPL-Cys
a2N-06	92-127	36	Bio-KHVLEMQEQLQKLEVELREVTKNKEKLRKNLLELVE-Cys
a2N-07	128-145	18	Bio-YTHMLRVTKTFLKRNVEF-Cys
a2N-08	146-163	18	Bio-EPTYEEFPALENDSLLDY-Cys
a2N-09	164-180	17	Bio-SCMQRLGAKLGFVSGLI-Cys
a2N-10	181-197	17	Bio-QQGRVEAFERMLWRACK-Cys
a2N-11	198-214	17	Bio-GYTIVTYAELDECLEDP-Cys
a2N-12	215-230	16	Bio-ETGEVIKWYVFLISFW-Cys
a2N-13	231-246	16	Bio-GEQIGHKVKKICDCYH-Cys
a2N-14	247-262	16	Bio-CHIYPYPNTAEERREI-Cys
a2N-15	263-278	16	Bio-QEGLNTRIQDLYTVLH-Cys
a2N-16	279-295	17	Bio-KTEDYLRQVLCKAAESV-Cys
a2N-17	296-312	17	Bio-CSRVVQVRKMKAIYHML-Cys
a2N-18	313-331	19	Bio-NMCSFDVTNKCLIAEVWCP-Cys
a2N-19	332-349	18	Bio-EVDLPGLRRALEEGSRES-Cys
a2N-20	350-367	18	Bio-GATIPSFMNTIPTKETPP-Cys
a2N-21	368-385	18	Bio-TLIRTNKFTEGFQNIVDA-Cys
a2N-22	386-402	17	Bio-YGVGSYREVNPALFTII-Cys

Fig. 1. Design and synthesis of a2N-derived peptides. a) Design of a2N-derived peptides according to their secondary structure predicted by PSIPRED and COILS software. The α-helices are shown as green cylinders, β-strands are shown as yellow arrows. b) Names, position, length and sequence of a2N-derived peptides. Bio — biotin-tag. Cys — cysteine. The interacting peptides are indicated in red and non-interacting peptides are in black.

The peptide pull-down experiments demonstrated a specific interaction of GST-ARNO(wt) with six of the a2N-derived peptides (a2N-01, a2N-03, a2N-11, a2N-12, a2N-18 and a2N-22) (Fig. 2a). The other 16 peptides, including a2N-06, which represents the putative CC-domain of a2N, did not bind to GST-ARNO(wt). The specificity of the GST-ARNO(wt) interaction was further confirmed using a GST-only construct as a control in the a2N-derived peptide pull-down assay (Fig. 2b). In order to confirm the involvement of multiple sites on a2N in the interaction with ARNO, we also used a recombinant protein pull-down assay. For this purpose a2N was divided into two parts: i) a2N-N (or $a2N_{1-133}$), the N-terminal part which contains sequence covered by the peptides from a2N-01 to a2N-06; and ii) a2N-C (or $a2N_{134-393}$), the C-terminal part which contains sequence covered by the peptides from a2N-07 to a2N-22. *In vitro* translated a2N-N and a2N-C mutants were used in pull-down experiments with purified GST-ARNO(wt) and demonstrated that both parts of a2N could interact with wild-type ARNO (Fig. S1). Thus, our data indicate that while multiple interaction motifs of a2N are involved in the interaction with ARNO, its predicted CC-domain does not appear to be involved in this process.

3.2. Homology modeling of human ARNO and mapping the binding sites on ARNO that are involved in interaction with a2N

Cytohesin family members including ARNO contain the following distinct domains: i) CC-domain (CC, brown); ii) Sec7-domain (Sec7, yellow); iii) PH-domain (PH, green) and iv) PB-domain (PB, blue) as well as linkers: v) Sec7 and PH-linker domains (LK, magenta) and vi) PH and PB-linker domains (white) (Fig. 3a) [33,44]. In order to properly define boundaries between these domains and regulatory elements, homology modeling of ARNO was performed. A spatial structure of human ARNO without the N-terminal CC region was made using the crystal structure of the autoinhibited form of Grp1 (also called ARNO3 or cytohesin-3) (PDB ID: 2R09) as a template (Fig. 3b) [32]. For 3D-structure, see also Supplementary information, Movie S1. In order to model full-length ARNO, the C-terminal domain of the human EB1 protein (PDB ID: 2HKQ, chain A) was used as a template for the CC-domain of ARNO. Some dihedral angles in the chimeric template were manually edited in SWISS-PDB Viewer [45] to avoid steric clashes. Energy minimization in Gromacs [46] was performed for equilibration of the template. The final models were built with Modeller9v2 [42] (Fig. 3). For 3D-structure, see also Supplementary information, Movie S2. Domains and structural elements of ARNO are colored and their amino acid positions are indicated as in Fig. 3a.

To examine the ability of these well-defined and functionally distinct domains of ARNO to interact with a2N, we cloned full-length ARNO(wt) and its four domains separately for bacterial expression of recombinant proteins (Fig. 4a). The Sec7/PH-linker region (242–261aa) was divided between the Sec7-domain and the PH-domain, while the PH/PB-linker region (375–379aa) was cloned as a part of the PH-domain (Fig. 3a). Interaction of a2N with full-length ARNO(wt) was used as a control in

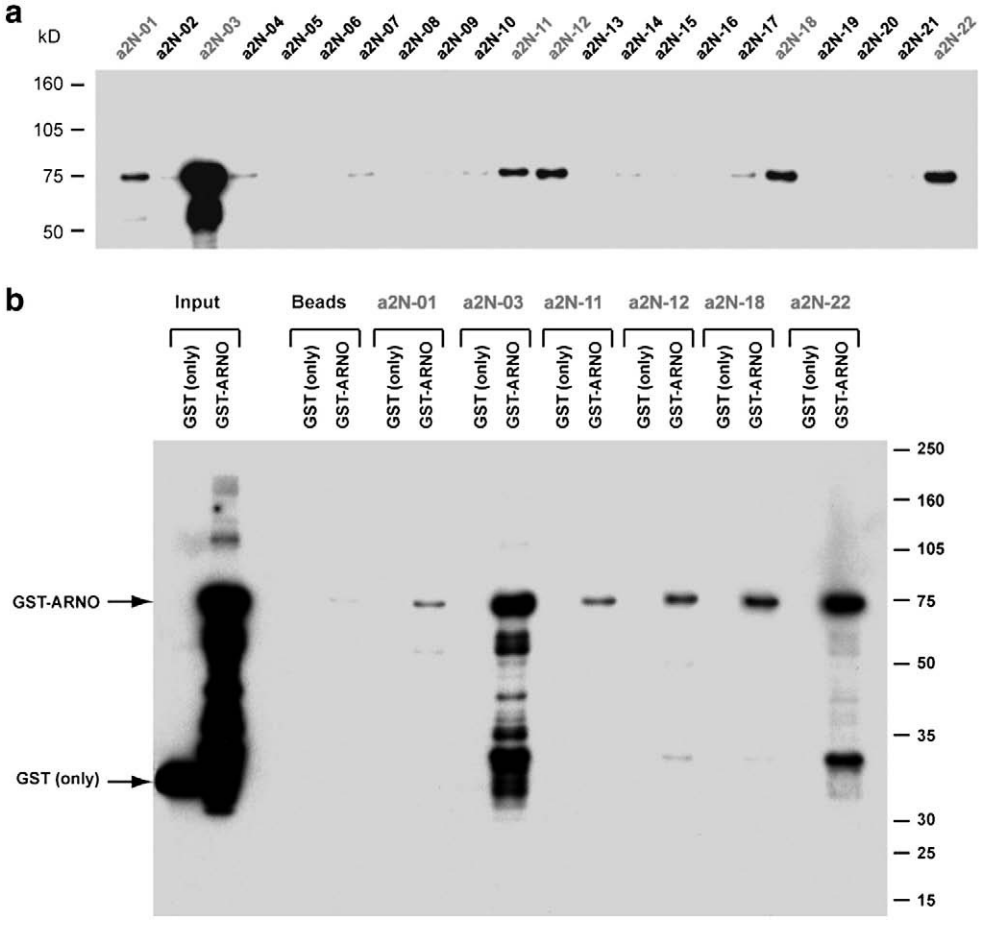

Fig. 2. Interaction of a2N with ARNO is mediated by multiple sites. a) a2N-derived peptide pull-down assay. The indicated a2N-derived peptides were immobilized on streptavidin-beads and incubated with purified recombinant GST-ARNO(wt). Interacting complexes were eluted and analyzed by Western blotting using monoclonal anti-GST antibodies as described in Materials and methods. The interacting peptides are indicated in red and non-interacting peptides are in black. b) Pull-down assay with selected a2N-derived interacting peptides incubated with either GST (negative control) or GST-ARNO(wt). The first two lanes show the patterns obtained when either GST-only (lane 1) or GST-ARNO(wt) (lane 2) are loaded onto the gel. The a2N-derived peptides were used in pull-down assay as described above and shown specific interaction with GST-ARNO(wt) but not with GST-only.

these experiments. These purified recombinant proteins (Fig. 4a) were used as baits in GST pull-down experiments with *in vitro* translated recombinant a2N as a prey. Interacting proteins were detected by western blot analysis with a2-specific antibodies as described in Materials and methods. Our data demonstrated that a2N interacts strongly with the ARNO Sec7-domain and weakly with its PH-domain, while no interaction with either the CC-domain or the PB-domain of ARNO could be detected (Fig. 4b). In order to determine whether the Sec7/PH-linker region itself could interact with a2N, we synthesized a peptide corresponding to the Sec7/PH-linker region (242–261aa) of ARNO (Figs. 3a and 5a), and we reproducibly observed an interaction of a2N with this linker region (Fig. 5b). Thus, our protein GST pull-down and peptide pull-down assays demonstrated that a2N strongly interacts with ARNO's catalytic Sec7-domain, while weak binding to the PH-domain and the linker between these two domains was also detected.

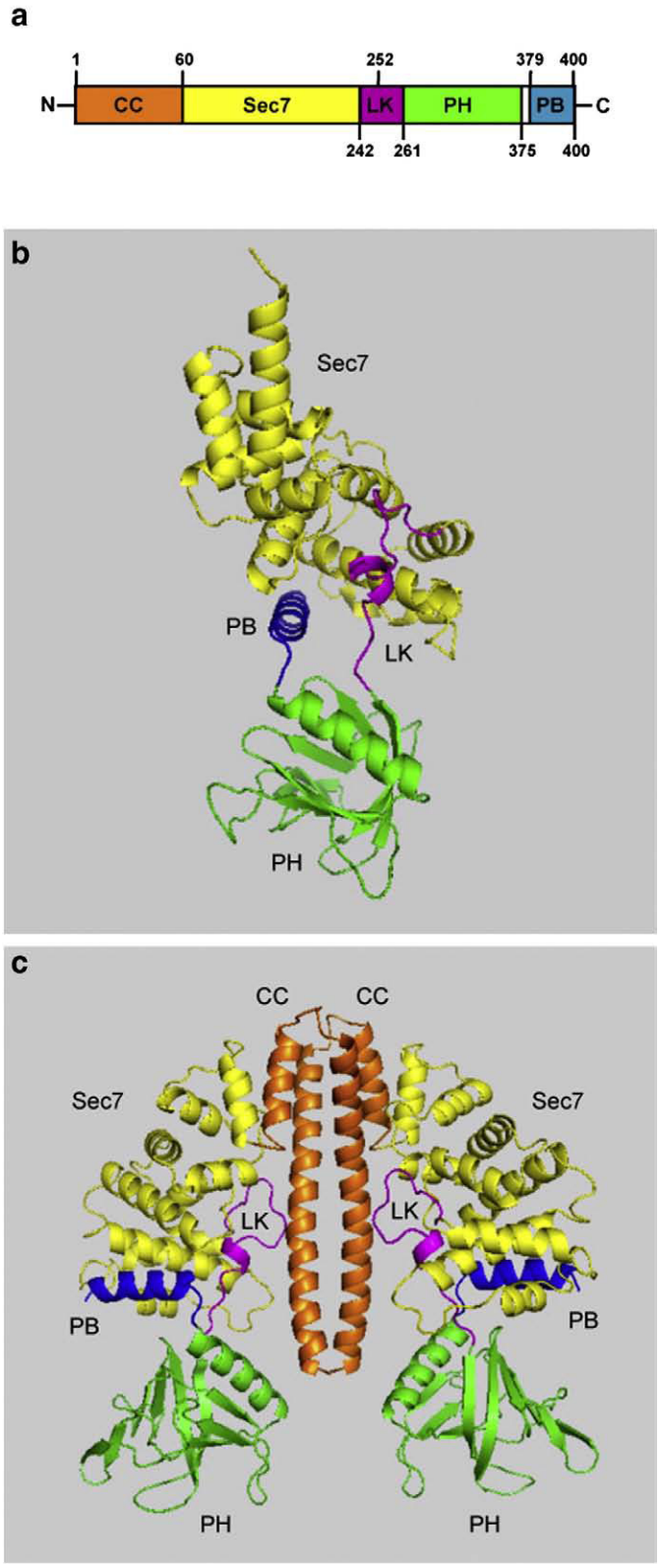

Fig. 3. Homology modeling of the structure of the autoinhibited ARNO. a) Schematic representation of domains and regulatory elements of ARNO. These structures are indicated as follows: i) CC-domain (1–60aa) in brown; ii) Sec7-domain (61–242aa) in yellow; iii) Sec-7-PH-linker (LK) (242–261aa) in magenta; iv) PH-domain (262–375aa) in green; v) PB-domain (376–400aa) in blue. Boundaries of the domains are indicated as amino acid numbers. b) Ribbon representations of a molecular model of delCC-ARNO in its monomeric and autoinhibited state. The autoinhibited model of ARNO without its CC-domain was performed based on the crystal structure of GRP1 (PDB ID: 2R09). Details are described in Results. Structural domains and elements of delCC-ARNO are indicated as in a. For 3D-structure see also Supplementary information, Movie S1. c) Ribbon representation of a molecular model of full-length ARNO(wt) in its dimeric and autoinhibited state. In order to model full-length ARNO(wt), the C-terminal domain of human EB1 protein (PDB ID: 2HKQ, chain A) was used as a template for the CC-domain of ARNO while the crystal structure of GRP1 (PDB ID: 2R09) was used as a template for the Sec7/PH/PB-domains. Details are described in Results. Structural domains and elements of delCC-ARNO are indicated as in a. For 3D-structure see also Supplementary information, Movie S2.

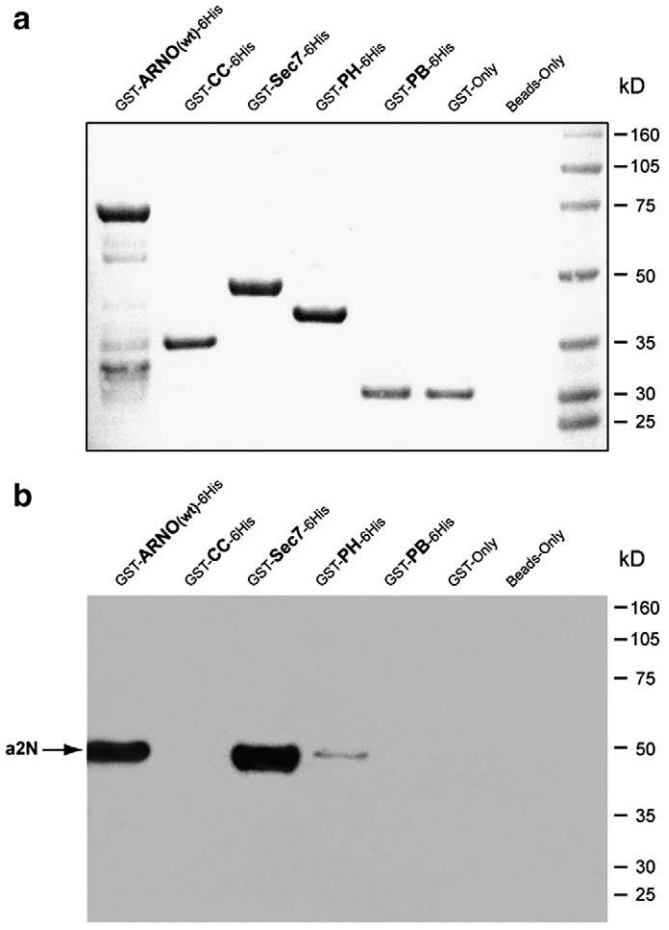

Fig. 4. Cytosolic tail of a2-subunit isoform of V-ATPase interacts strongly with Sec7-domain and weakly with PH-domain of ARNO. a) Purity of GST and 6His double-tagged ARNO(wt) and its domains used in GST pull-down experiments. Proteins were resolved by Nu-PAGE and stained by Ponceau-S. Molecular weight markers are shown on the right. b) The amount of a2N pulled-down by each fusion protein was analyzed by Western blotting using specific anti-a2N antibodies. Wild-type ARNO(wt) and its Sec7-domain showed strong binding with a2N in this assay. Weak interaction of a2N with PH-domain could also be detected. Molecular weight markers are shown on the right.

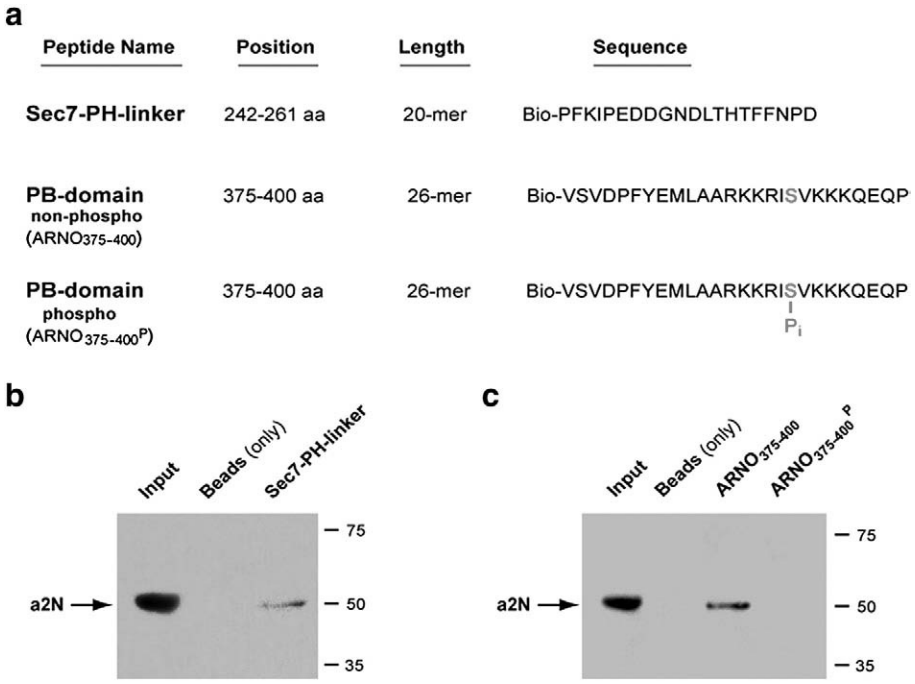

Fig. 5. Phosphorylation-dependent interaction of a2N with PB-domain of ARNO. a) Names, position, length and sequence of synthetic ARNO-derived peptides are shown as follows: i) Sec7-PH-linker; ii) non-phosphorylated PB-domain ($ARNO_{375–400}$) and iii) phosphorylated PB-domain domain ($ARNO_{375–400}^{P}$). Serine392 (Ser_{392}) of ARNO the substrate for PKC-dependent phosphorylation is indicated in red. b) Peptide pull-down assay showing interaction of a2N with Sec7-PH-linker of ARNO. c) Phosphorylation-dependent interaction of a2N with ARNO-derived peptide corresponding to the PB-domain of ARNO. Corresponding ARNO-derived peptides were immobilized on streptavidin-beads and incubated with *in vitro* translated recombinant a2N. Interacting complexes were eluted and analyzed by Western blotting using anti-a2N antibodies.

3.3. Phosphorylation-dependent interaction of a2N with the regulatory PB-domain of ARNO

Next we tested whether: i) interaction of a2N with the PB-domain (379–400aa, short 22 amino acids construct) was prevented by the addition of two tags (bulky 26 kDa GST-tag and His-tag) on the ARNO construct (Fig. 4b) and ii) whether this interaction could be modified by Ser_{392} phosphorylation of the PB-domain of ARNO. Thus, we synthesized a biotinylated peptide called $ARNO_{375–440}$ which covers the PB-domain (379–440aa) and also includes four additional amino acids of a PH/PB-linker (375–378aa) (Figs. 3a and 5a). Also a phosphorylated version of this peptide $ARNO_{375–440}^{P}$ (Ser_{392}-residue is known to be phosphorylated by PKC *in vivo*) was synthesized (Fig. 5a) [34]. Using these peptides in pull-down experiments, a direct interaction of a2N with non-phosphorylated $ARNO_{375–400}$ was demonstrated (Fig. 5c). Importantly, this interaction was specific since interaction between a2N and $ARNO_{375–400}^{P}$ it was completely abolished by Ser_{392}-phosphorylation (Fig. 5c).

3.4. Structural changes of the $ARNO_{375–400}$ peptide caused by its Ser_{392}-phosphorylation

In order to understand the phosphorylation-dependent mechanism of interaction between a2N and ARNO-derived peptides, the structural traits of the non-phosphorylated ($ARNO_{375–400}$) and phosphorylated ($ARNO_{375–400}^{P}$) peptides were determined by solution NMR spectroscopy. All amino acids of the two peptides were sequentially assigned. The connectivity diagrams of $ARNO_{375–400}$ (see Supplementary information, Fig. S2a–e) and $ARNO_{375–400}^{P}$ (see Supplementary information, Fig. S3a–e) respectively, are indicative of a helical conformation with the sequential HN–HN, Ha–HN($i, i+3$), Ha–HN($i, i+4$), and Ha–Hb($i, i+3$) connectivities. Data from assigned 2D NOESY spectra and primary amino acid sequence were used as input for the automated structure calculation using the Cyana 2.1 package [38]. In total, an ensemble of twenty calculated structures resulted in an overall mean root square deviation (RMSD) of 0.69 Å for non-phosphorylated $ARNO_{375–400}$ (Fig. 6a) (PDB ID: 2kpa and BMRB ID: 16550) and 0.378 Å for $ARNO_{375–400}^{P}$ (Fig. 6b) (PDB ID: 2kpb and BMRB ID:16551). For 3D-structures see also Supplementary information Movie S3 and Movie S4. All these structures have energies lower than -100 kcal mol^{-1}, no NOE violations greater than 0.3 Å and no dihedral violations greater than 5°. Summary of the statistics for twenty structures are shown in the table (see Supplementary information, Fig. S5). The calculated structure $ARNO_{375–400}$ forms a stable N-terminus region with a helix extending from 378 to 384, followed by a short loop from 385 to 387, a second helix between 388 and 391 and a third very unstable 3_{10} helix from 394 to 397 (Fig. 6a). The remaining C-terminal amino acids form a flexible structure. Structural regions of $ARNO_{375–400}$ are also reflected in the NOE plot (see Supplementary information, Fig. S2). Electrostatic potential surface analysis showed that the peptide is strongly basic in nature, reflecting its name, the polybasic (PB) domain of ARNO (Supplementary information, Fig. S4) [34]. By comparison the structural assignment and calculation of $ARNO_{375–400}^{P}$, showed an N-terminus α-helix extending from residues 377–384 and a second α-helix at the C-terminus composed of residues 390–396, forming together a stable helix–loop–helix structure with a RMSD value of 0.378 Å (Fig. 6b) (see Supplementary information, Fig. S3). The loop between the two α-helices extends from residues 385–389. Superimposition of both structures, $ARNO_{375–400}$ and $ARNO_{375–400}^{P}$ (Fig. 6c) via N-terminus 1–10 residues revealed a nice fitting in this region with a root mean square deviation of 0.68 Å but with difference in the C-terminus. An alignment of the structures at the N-termini resulted in a distance deviation of 105° between the two C-termini at the loop region of $ARNO_{375–400}$ and $ARNO_{375–400}^{P}$, respectively. Thus, the Ser_{392}-phosphorylation of $ARNO_{375–400}$ peptide produced significant structural changes in the C-terminus, resulting in the disruption of the α-helix at the Ser_{392} residue in the non-phosphorylated $ARNO_{375–400}$. In contrast, $ARNO_{375–400}^{P}$ displayed an extended helix through Ser_{392} and attained a maximum stable structure (Fig. 6c). These structural changes could be responsible for the inhibitory effect of Ser_{392}-phosphorylation

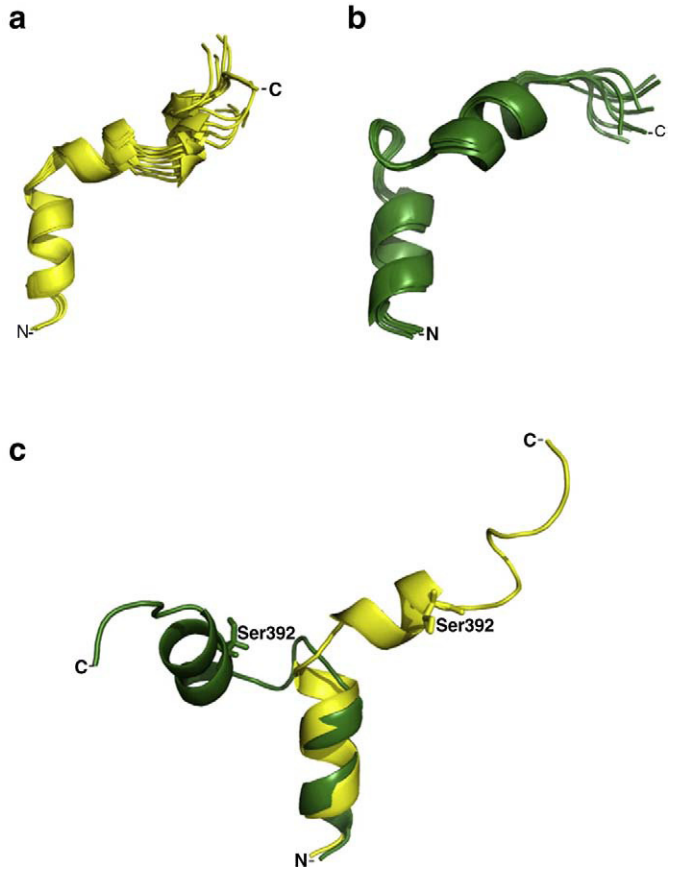

Fig. 6. Phosphorylation-dependent conformational changes of $ARNO_{375–400}$ and $ARNO_{375–400}^{P}$ peptides. a) Ribbon representation for the NMR structure of the peptide $ARNO_{375–400}$ (PDB ID: 2kpa and BMRB ID: 16550) corresponding to non-phosphorylated PB-domain of ARNO. Superimposition of the ten lowest energy structures of the peptide $ARNO_{375–400}$ is shown in yellow. For 3D-structure see Supplementary information, Movie S3. b) Ribbon representation for the NMR structure of the peptide $ARNO_{375–400}^{P}$ (PDB ID: 2kpb and BMRB ID: 16551) corresponding to phosphorylated PB-domain of ARNO. Superimposition of the ten lowest energy structures of the peptide $ARNO_{375–400}^{P}$ is shown in green. For 3D-structure see Supplementary information, Movie S4. c) Superimposition of the average structure $ARNO_{375–400}$ (yellow) and $ARNO_{375–400}^{P}$ (green) showing the different angle between the helices in both structures due to phosphorylation of the Ser_{392} of the PB-domain of ARNO. For assignment of cross-peaks in the NOESY spectrum of $ARNO_{375–400}$ and $ARNO_{375–400}^{P}$ peptides see Supplementary information, Figs. S1 and S2. For assignment 3D NMR of $ARNO_{375–400}$ and $ARNO_{375–400}^{P}$ peptides see Supplementary information, Figs. S3A and S3B. For statistics of NMR data of $ARNO_{375–400}$ and $ARNO_{375–400}^{P}$ peptides see Supplementary information, Fig. S4.

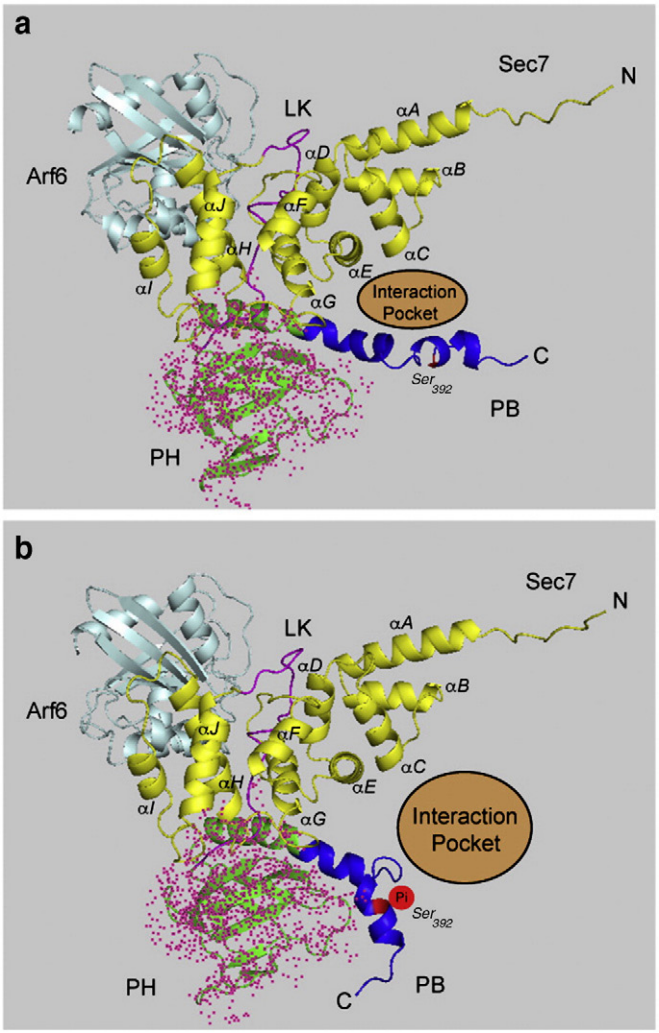

Fig. 7. Homology modeling of activated ARNO and conformational changes caused by phosphorylation of Ser_{392} in its PB-domain. a) Ribbon representation of a molecular model of non-phosphorylated ARNO in its activated state in a complex with Arf6. Modeling was performed by superimposition of the known structure of the Sec7-domain of ARNO in a complex with Arf1 (PDB ID: 1S9D) onto a delCC-ARNO/Arf6 model as described in Results. The PH-domain was shadowed to indicate its arbitrary position. Structure of non-phosphorylated peptide $ARNO_{375–400}$ (see Fig. 6a) was used as a template of non-phosphorylated PB-domain (in blue). Position of Ser_{392} on the ARNO PB-domain is shown in red. Molecular model of Arf6 is shown in cyan, while other domains and structural elements of ARNO are colored as in Fig. 3a. Ten helices of the Sec7-domain are numbered and indicated correspondingly from αA to αJ as previously described [32,51]. For 3D-structure see Supplementary information, Movie S5. b) Ribbon representation of a molecular model of phosphorylated ARNO in its activated state in a complex with Arf6. Modeling was performed by superimposition of the known structure of the Sec7-domain of ARNO in a complex with Arf1 (PDB ID: 1S9D) onto a delCC-ARNO/Arf6 model as described in Results. The PH-domain was shadowed to indicate its arbitrary position. Structure of phosphorylated peptide $ARNO_{375–400}^{P}$ (see Fig. 6b) was used as a template of phosphorylated PB-domain (in blue). Phosphorylated Ser_{392} residue is shown in red. Molecular model of Arf6 is shown in cyan, while other domains and structural elements of ARNO are colored as in Fig. 3a. Ten helices of the Sec7-domain are indicated correspondingly from αA to αJ as previously described [32,51]. For 3D-structure see Supplementary information, Movie S6.

on $ARNO_{375–400}$ interaction with a2N observed in our peptide pull-down experiments (Fig. 5c) as discussed below.

3.5. Homology modeling of ARNO conformational changes caused by Ser_{392}-phosphorylation of its PB-domain

A spatial structure of human ARNO without the N-terminal CC region was derived using homology modeling as described above. The crystal structure of the autoinhibited form of Grp1 (PDB ID: 2R09) was also used as a template and the model was built using Modeller9v2 software [42]. A spatial model of activated ARNO is shown in a complex with Arf6 and the structure was equilibrated in Gromacs (Figs. 7a,b) [46]. Nucleotide exchange on both Arf6 and Arf1 is activated by the Sec7-domain of ARNO. Superimposition of the known crystal structure of the human Sec7–Arf1 complex onto ARNO with Arf6 shows that the PH-domain and Arf6 occupy the same space (Fig. S6). Thus, Arf6 binding may take place only concurrently with conformational changes in ARNO. First, since the exact relative positions between the Sec7 and PH-domains in activated cytohesins is currently unknown, during this step the PH-domain in the ARNO model was manually moved to a position that allows binding of Arf6 (Figs. 7a,b). To indicate its arbitrary position in this model, the PH-domain has been shadowed (Figs. 7a,b). During the second step, the NMR structure of non-phosphorylated peptide $ARNO_{375–400}$ (Fig. 6a) (PDB ID: 2kpa and BMRB ID:16550) was used for modeling of the non-phosphorylated PB-domain in the ARNO model (Fig. 7a). For 3D-structures, see also Supplementary information, Movie S5. On

the other hand, the NMR structure of the phosphorylated peptide $ARNO_{375-400}^{P}$ (Fig. 6b) (PDB ID: 2kpb and BMRB ID: 16551) was used for modeling of the phosphorylated PB-domain in the ARNO model (Fig. 7b). For 3D-structures, see also Supplementary information, Movie S6. These modeling studies revealed the existence of a potential interaction pocket that is formed by the αC, αE and αG helices of the Sec7-domain and two semi-helices of the PB-domain of activated ARNO (Fig. 7a). This model also predicted that conformational changes caused by Ser_{392}-phosphorylation could result in the opening of this interaction pocket and, thus, modifies its binding interfaces on both Sec7 and PB-domains of ARNO (Fig. 7b). Therefore, we next performed experiments designed to identify the specific part of the a2N that may potentially be involved in the binding within this interaction pocket.

3.6. Identification of a motif on a2N that is involved in specific binding with the Sec7-domain of ARNO

In order to map the motif(s) on a2N that interact with the Sec7-domain of ARNO, the peptide pull-down approach was also applied using six of the a2N-derived ARNO-interacting peptides (a2N-01, a2N-03, a2N-11, a2N-12, a2N-18 and a2N-22). The peptides were immobilized on streptavidin-beads and incubated with purified recombinant GST-only or GST-Sec7-domain. These experiments demonstrated that only two peptides a2N-01 and a2N-03 interact with the catalytic Sec7-domain of ARNO (Fig. 8a). Next, we tested the specificity of binding of these two peptides to Sec7 in comparison to other domains of ARNO. These pull-down experiments demonstrated that peptide a2N-01 ($a2N_{1-17}$, MGSLFRSESMCLAQLFL) showed

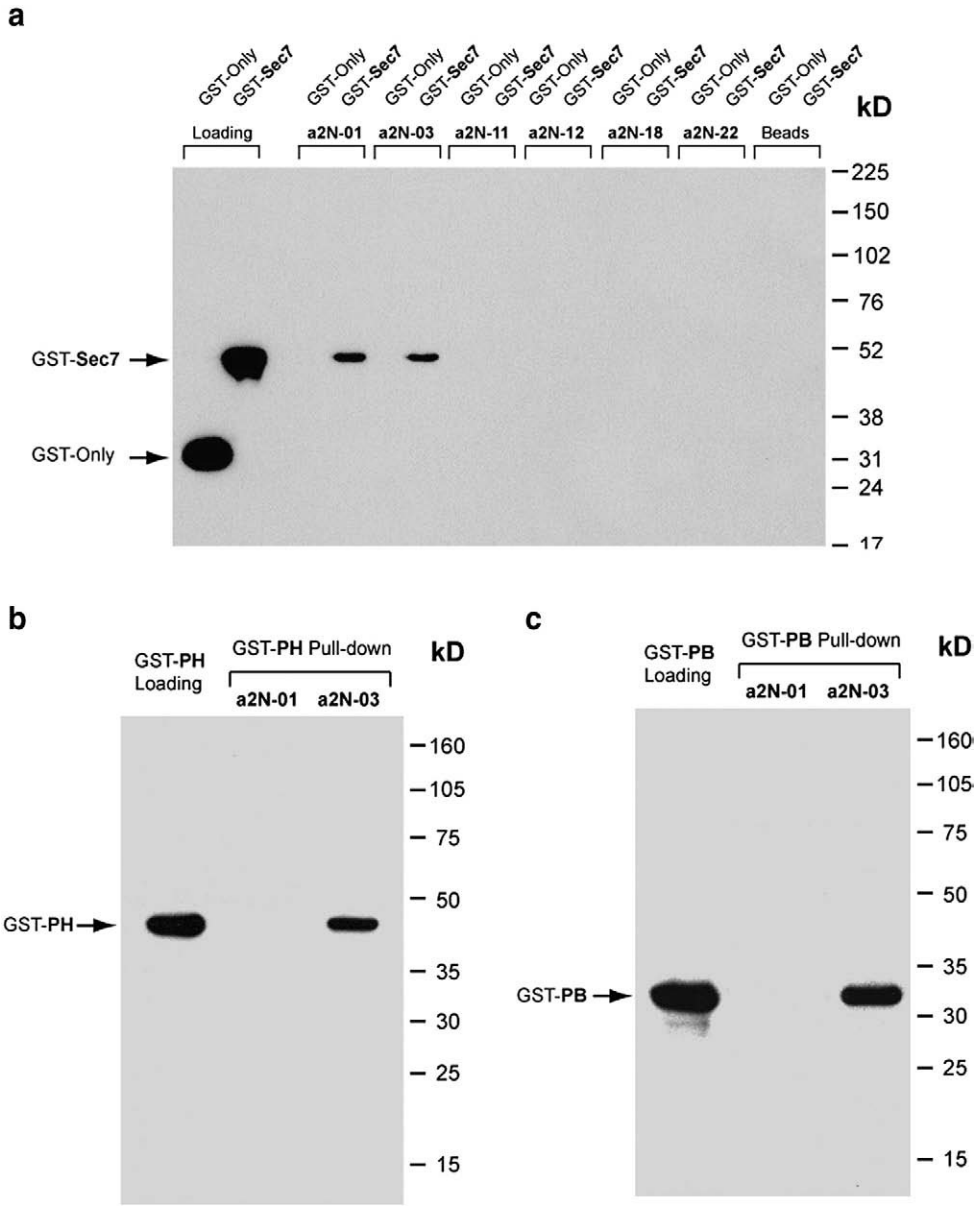

Fig. 8. Identification of interaction motif of a2N that is involved in specific binding with the Sec7-domain of ARNO. a) Catalytic Sec7-domain of ARNO interacts with two a2N-derived peptides a2N-01 and a2N-03 in pull-down experiments. The peptide pull-down assay was performed with six a2N-derived interaction peptides immobilized on streptavidin-beads and incubated with purified recombinant GST-only or GST-Sec7-domain. Interacting complexes were eluted and analyzed by Western blotting using monoclonal anti-GST antibodies as described in Materials and methods. The loading controls for GST-only (lane 1) or GST-Sec7 (lane 2) are shown. b,c) Peptide a2N-01 specifically interacts with Sec7 but not PH-domain (b) or PB-domain (c) of ARNO. The peptide pull-down assay was performed with peptides a2N-01 and a2N-03 immobilized on streptavidin-beads and incubated with purified recombinant GST-PH-domain (b) or GST-PB-domain (c). Interacting complexes were eluted and analyzed by Western blotting using monoclonal anti-GST antibodies as described in Materials and methods. The loading control of GST-PH-domain (b) or GST-PB-domain (c) is shown on the left.

specificity towards Sec7-domain and did not interact with either the PH-domain (Fig. 8b) or with the PB-domain (Fig. 8c) of ARNO. On the other hand, peptide a2N-03 lacks this specificity and interacts equally well with both the PH-domain (Fig. 8b) and PB-domain (Fig. 8c) of ARNO.

3.7. Estimation of the binding affinities using surface plasmon resonance analysis

To determine the dissociation constants (K_D) for binding of a2N(wt)/ARNO(wt) proteins and for the specific peptide a2N-01/Sec7-domain interaction, a kinetic analysis was performed using the BIAcore™ T100 system as described in Materials and methods. Specific concentration-dependent responses were obtained for both interactions (Fig. 9). When various concentrations of His6-ARNO(wt) were applied to a2N-His6(wt) immobilized on a sensor chip, a specific real-time binding between the two proteins was observed (Fig. 9a). The best fitted curves with bivalent analyte interaction isotherms were obtained and calculation of K_D was performed using the BIAcore™ T100 Evaluation software. An association rate constant (k_{on}) of 4.77×10^3 M^{-1} S^{-1} was obtained and a dissociation rate constant (k_{off}) of 14.95×10^{-4} S^{-1} was determined, giving a dissociation constant of K_D (k_{off}/k_{on}) for this interaction of $K_D = 3.13\times10^{-7}$ M. The kinetic analysis and estimation of K_D for the a2N-01/Sec-7 interaction was also calculated using a2N-01 peptide immobilized as ligand on the sensor chip, with various concentrations of Sec7-domain as analytes (Fig. 9b). The best fitted curve was a single 1:1 interaction isotherm and k_{on} was determined as 2.5×10^3 M^{-1} S^{-1} and k_{off} was determined as 8.6×10^{-4} S^{-1} with a calculated K_D for this interaction of 3.44×10^{-7} M. For both interactions, association rates were fast and dissociation rates were slow, which resulted in the formation of a relatively stable complex that was readily detectable in our pull-down (Figs. 2a,b and 8a) and previous immunoprecipitation experiments [1]. Calculated free energies for a2N(wt)/ARNO(wt) and a2N-01/Sec7 binding are −8.86 kcal mol^{-1} and −8.81 kcal mol^{-1}, respectively [35]. These equivalent free energies strongly indicate that specific binding between peptide a2N-01 in the a2N and the Sec7-domain of ARNO is most likely one of the major contributors to the high-affinity interaction between a2N and ARNO.

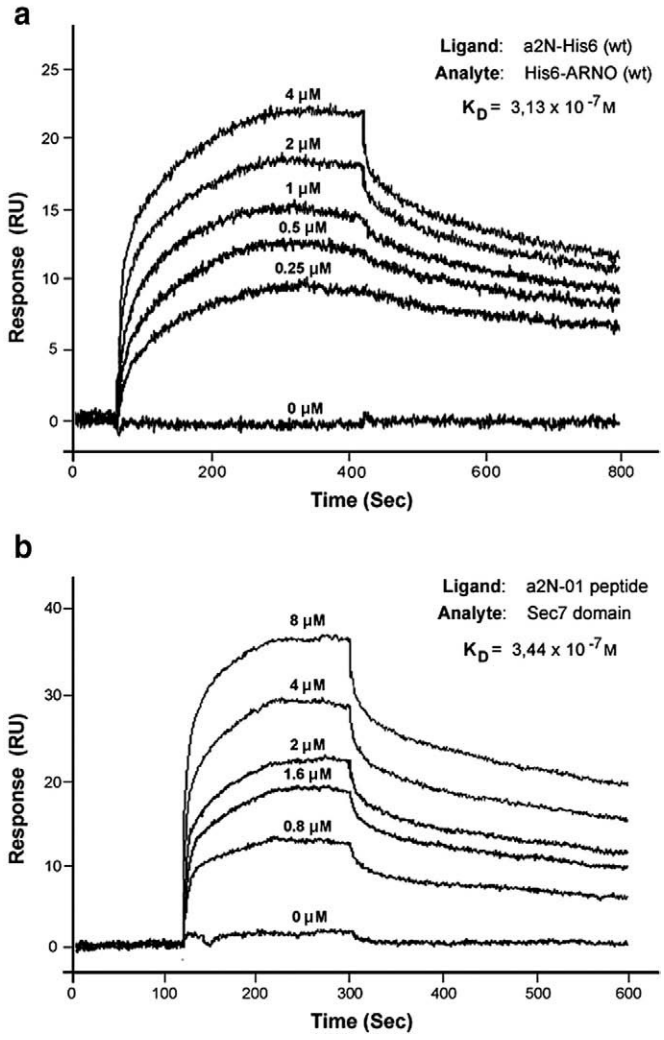

Fig. 9. Estimation of the binding affinities for the specific interaction domains between V-ATPase a2-subunit isoform and ARNO. a) Kinetic analysis and estimation of a dissociation constant (K_D) for interaction between full-length a2N(wt) and ARNO(wt) proteins. Sensorgrams for the binding of recombinant a2N-His6 immobilized as ligand on the sensor chip, with various concentrations of His6-ARNO as analyte are shown. The responses on the sensorgram are designated in resonance units (RU). The best fitted curves with bivalent analyte interaction isotherm were obtained and the $K_D = 3.13\times10^{-7}$ M value was determined using BIAcore™ T100 evaluation software. b) Kinetic analysis and estimation of K_D for interaction between a2N-01 peptide and Sec7-domain of ARNO. Sensorgrams for the binding of a2N-01 peptide immobilized as ligand on the sensor chip, with various concentrations of Sec7-domain as analyte are shown. The responses on the sensorgram are designated in resonance units (RU). The best fitted curves with single 1:1 interaction isotherm were obtained and the $K_D = 3.44\times10^{-7}$ M value was determined using BIAcore™ T100 evaluation software.

4. Discussion

We previously showed that the V-ATPase functions as an endosomal pH-sensor that recruits Arf6 and ARNO to the endosomal membrane and provides a regulatory link between intra-endosomal acidification and protein trafficking in the endosomal/lysosomal protein degradative pathway [1,2]. While the a2-subunit isoform of the V-ATPase is targeted to early endosomes and directly interacts with ARNO in an acidification-dependent manner, Arf6 specifically interacts with the c-subunit of the V-ATPase. However, the molecular mechanism(s) underlying these novel interactions of the V-ATPase and their precise effects on downstream signaling pathways remain obscure. In this study, we set out to identify the cognate binding motifs on the a2-subunit isoform of V-ATPase and ARNO in order to begin to understand how their interaction might be modulated.

First, we mapped the entire a2N in order to uncover the motifs that are involved in binding with wild-type ARNO. Recombinant protein pull-down assays with a2N-N (corresponding to the N-terminal part of $a2N_{1-133}$) and with a2N-C (corresponding to the C-terminal part of $a2N_{134-393}$) suggested the involvement of multiple sites that participate in the a2N/ARNO interaction. The peptide pull-down experiments also revealed the interaction of ARNO(wt) with six (a2N-01, a2N-03, a2N-11, a2N-12, a2N-18 and a2N-22) out of the twenty two a2N-derived peptides. Taken together, these data demonstrate that both N-terminal and C-terminal parts of the a2N are competent for binding with ARNO and multiple binding sites located on both portions of the a2N are involved in the interaction with ARNO.

Next, using the recently published crystal structure of GRP1 or cytohesin-3 as a template [32], we applied a homology modeling approach and generated the following 3D-structures for ARNO: i) the dimeric form of full-length ARNO(wt) and ii) the monomeric form of delCC-ARNO without its CC-domain. While the CC-domain of ARNO is involved in binding to the CASP protein [47] our present and previous [1] data indicated that it does not interact with a2N. It is, however, generally accepted that the CC-domain of ARNO is involved in its homo-dimerization [44] and it may have a regulatory role in binding of ARNO with a2N. Indeed, our previous data demonstrated that removal of the CC-domain from ARNO increased the interaction of delCC-ARNO with the a2N [1]. Importantly, we demonstrated that peptide a2N-06 corresponding to a putative CC-domain of the a2N does not interact with ARNO. Thus, binding of ARNO with a2N is not a

simple hetero-dimerization involving their respective CC-domains, but rather is a complex and dynamic process involving multiple interaction sites on both a2N and ARNO.

Our study revealed that the V-ATPase a2-subunit isoform interacts with the following domains and structural elements of ARNO: i) catalytic Sec7-domain; ii) lipid-binding plekstrin-homology (PH) domain; iii) linker element between these domains (Sec7-PH-linker) and iv) polybasic (PB) domain. The interaction of a2N with the Sec7-domain of ARNO in pull-down experiments is quite strong and is comparable to the interaction of a2N with full-length ARNO. In order to identify the motif of a2N that is involved in specific binding with the ARNO Sec7-domain, some additional pull-down experiments with a2N-derived interacting peptides and the Sec7-domain of ARNO were performed. We demonstrated that only two of the six identified a2N-derived interacting peptides a2N-01 and a2N-03 could interact with the Sec7-domain of ARNO. However, and importantly, only the a2N-01 ($a2N_{1-17}$, MGSLFRSESMCLAQLFL) peptide showed specificity towards the Sec7-domain.

It is known that some synthetic peptides in solution may exert strong but non-specific interactions. However, in context of the whole intact protein, the motifs formed by these peptides may be shielded and never be available for such potential interactions. This situation may lead to an over-estimation of binding capacity and false-positive results in experiments with synthetic peptides in solution. Indeed, we suggest that this is the case with peptide a2N-03, since it interacts equally strongly and not specifically with wild-type ARNO and its Sec7-, PH- and PB-domains only in solution (Figs. 2 and 8). However, the whole intact a2N reveals a predominant specificity towards the ARNO Sec7-domain (Fig. 4). Thus, we hypothesize that in the context of the properly folded a2-subunit isoform, the motif formed by peptide a2N-03 is probably completely shielded by other parts of the protein, which prevents its interaction with ARNO. We anticipate that future structural studies on the a2N-subunit isoform will reveal the exact location of this a2N-03 motif within the full-length protein.

It is also possible that some synthetic peptides in solution may not necessary acquire the same conformation as their counterparts in the intact protein. Thus, they may not precisely reflect the affinity of interactions with their binding partners that would occur in the micro-environment of the whole protein. This situation would produce an underestimation of binding capacity or even false-negative results in binding experiments with synthetic peptides. Therefore, the qualitative peptide binding assays need to be confirmed by quantitative methods such as the BIAcore assay using both synthetic peptides and recombinant proteins. In the present study, surface plasmon resonance studies confirmed results from our pull-down experiments by showing specific, high-affinity, real-time binding kinetics of the a2N-01 peptide with ARNO's Sec7-domain. These data strongly suggest that these motifs are most likely to form the predominant interaction site between these two proteins. Additional evidence for an important role of the ARNO Sec7-domain in the V-ATPase interaction comes from a recent study showing a direct involvement of the Sec7-domain of the Gea2p protein (another Arf-GEF) in interaction with Drs2p (a P-type ATPase) in yeast [48].

While a2N strongly interacts with the Sec7-domain, it binds only weakly to the PH-domain of ARNO. A recent study revealed that a stretch of twenty amino acids between the Sec7 and PH-domains, called the Sec7-PH-linker (242–261aa), is an important regulatory element in auto-regulation and activation of the GEF activity of ARNO [32]. Using a synthesized Sec7-PH-linker in peptide pull-down experiments we were able to demonstrate a direct interaction of a2N with this important regulatory element of ARNO. Thus, the relatively weak binding of the PH-domain with a2N could be attributed to the requirement of the Sec7-PH-linker for full interaction with the PH-domain. In addition, the PB-domain of the cytohesin-family has also been identified as a crucial regulatory element in auto-regulation and modulation of their Arf-GEF activity [32]. Here, we found that a2N also specifically interacts with the $ARNO_{375-400}$ peptide corresponding to the PB-domain of ARNO. Importantly, this interaction was completely abolished by phosphorylation of serine392 (Ser_{392}) in the $ARNO_{375-400}{}^{P}$ peptide. Here, for the first time, the three-dimensional structures of both non-phosphorylated ($ARNO_{375-400}$) and phosphorylated ($ARNO_{375-400}{}^{P}$) peptides were resolved by NMR. Homology modeling studies predicted dramatic conformational changes in the ARNO interaction pocket caused by Ser_{392}-phosphorylation. Although these peptides make up only a segment of ARNO, these conformational changes of the PB-domain may modulate the access and interaction of a2N with the Sec7-domain of ARNO.

Importantly, it is well known that PKC-dependent phosphorylation of Ser_{392} regulates the catalytic activity of ARNO. However, the molecular mechanism of this regulation remained undetermined [34]. Thus, the conformational changes of $ARNO_{375-400}$ and $ARNO_{375-400}{}^{P}$ peptides reported in our study could also explain the mechanism of regulation of the catalytic activity of ARNO by PKC-dependent Ser_{392}-phosphorylation [32,34]. In a recent study dealing with auto-regulation of the cytohesin protein family, very similar non-phosphorylated and phosphorylated synthetic peptides corresponding to the PB-domain of cytohesin-1 were covalently ligated to the cytohesin-1 (residues 53–377) recombinant protein [32]. These synthetic peptide/recombinant protein chimeras were functionally active, and while the phosphorylation of this peptide leads to activation of GEF activity of cytohesin-1, its dephosphorylation reverses this activation. Thus, this study also supports the validity and physiological relevance of our structural studies with similar peptides such as $ARNO_{375-400}$ and $ARNO_{375-400}{}^{P}$ as well as indicating the proper folding of these synthetic peptides in solution.

Recently, the dissociation constants for interactions between various subunits of the V-ATPase complex have been determined similarly using the BIAcore™ assay. For the subunits NtpI (homolog of mammalian a-subunit) and NtpF (homolog of mammalian G-subunit) of the V-ATPase from *Enterococcus hirae* the dissociation constant was $K_D = 1.9 \times 10^{-5}$ M, while for NtpF in complex with NptE (homolog of mammalian E-subunit) the $K_D = 1.5 \times 10^{-7}$ M [49]. While the dissociation constant of the binding between Vph1p (homolog of mammalian a-subunit) and VMA6 (homolog of mammalian *d*-subunit) was $K_D = 6.0 \times 10^{-8}$ M, a K_D of 2.7×10^{-7} M was determined for binding of VMA6 with VMA1 (homolog of mammalian A-subunit) in the yeast V-ATPase [50]. Thus, the affinity of interactions between a2N(wt)/ARNO(wt) and a2N-01/Sec7 that we find here are in the same range as those determined for interactions between subunits within V-ATPase complex itself, indicating an important cell biological role of the interaction between V-ATPase and small GTPase regulatory proteins.

In conclusion, we have found two structural elements that are involved in specific and high-affinity association of the V-ATPase a2-subunit isoform and ARNO: i) an N-terminal binding motif formed by the first seventeen amino acids of the a2N (MGSLFRSESMCLAQLFL) and ii) an interaction pocket formed by the catalytic Sec7 and regulatory PB-domains of ARNO. Our data also suggest that the transmembrane a2-subunit isoform of the V-ATPase may not simply recruit and scaffold small GTPases to their target membrane during its function as a pH-sensor [1]. Via its interaction with the catalytic Sec7-domain and with the regulatory elements of ARNO, it could also have a novel role as a modulator of Arf-GEF activity and ultimately as modulator of activity of Arf-family small GTPases. Such a suggested novel function of the V-ATPase as an Arf-GEF regulator remains to be tested in future studies.

Acknowledgements

We would like to thank Dr. Dennis Brown and Dr. Masamitsu Futai for the critical reading and constructive suggestions during the preparation of this manuscript. We also would like to thank Dr. Ashok Khatri, (Director of Partners/MGH Peptide/Protein Core Facility) for

the assistance with peptide synthesis. We are grateful to Dr. James Casanova for his generous gift of the cDNA construct of human ARNO. We are also grateful to S. Gayen, School of Biological Sciences, NTU, for the assistance in generating the NMR related figures. This study was supported by a National Institutes of Health (NIH) grant DK038452 and by Boston Area Diabetes Endocrinology Research Center (BADERC) grant DK057521-08 (to VM) as well as by the School of Biological Sciences, Nanyang Technological University (NTU) grant SUG/31/05 (to GG). Y.R. Thaker is grateful to the authority of NTU for awarding a research scholarship.

Appendix A. Supplementary data

Supplementary data associated with this article can be found, in the online version, at doi: 10.1016/j.bbabio.2010.02.009.

References

[1] A. Hurtado-Lorenzo, M. Skinner, J. El Annan, M. Futai, G.H. Sun-Wada, S. Bourgoin, J. Casanova, A. Wildeman, S. Bechoua, D.A. Ausiello, D. Brown, V. Marshansky, V-ATPase interacts with ARNO and Arf6 in early endosomes and regulates the protein degradative pathway, Nat. Cell Biol. 8 (2006) 124–136.
[2] V. Marshansky, The V-ATPase a2-subunit as a putative endosomal pH-sensor, Biochem. Soc. Trans. 35 (2007) 1092–1099.
[3] V. Marshansky, M. Futai, The V-type H(+)-ATPase in vesicular trafficking: targeting, regulation and function, Curr. Opin. Cell Biol. 20 (2008) 415–426.
[4] Z. Zhang, Y. Zheng, H. Mazon, E. Milgrom, N. Kitagawa, E. Kish-Trier, A.J. Heck, P.M. Kane, S. Wilkens, Structure of the yeast vacuolar ATPase, J. Biol. Chem. 283 (2008) 35983–35995.
[5] M. Diepholz, D. Venzke, S. Prinz, C. Batisse, B. Florchinger, M. Rössle, D.I. Svergun, B. Böttcher, J. Fethiere, A different conformation for EGC stator subcomplex in solution and in the assembled yeast V-ATPase: possible implications for regulatory disassembly, Structure 16 (2008) 1789–1798.
[6] S.P. Muench, M. Huss, C.F. Song, C. Phillips, H. Wieczorek, J. Trinick, M.A. Harrison, Cryo-electron microscopy of the vacuolar ATPase motor reveals its mechanical and regulatory complexity, J. Mol. Biol. 386 (2009) 989–999.
[7] D. Brown, V. Marshansky, Renal V-ATPase: physiology and pathophysiology, in: M. Futai, Y. Wada, J.H. Kaplan (Eds.), Handbook of ATPases. Biochemistry, Cell Biology, Pathophysiology, Wiley-VCH Verlag GmbH & Co. KGaA, Weinheim, 2004, pp. 413–442.
[8] C.A. Wagner, K.E. Finberg, S. Breton, V. Marshansky, D. Brown, J.P. Geibel, Renal vacuolar H+-ATPase, Physiol. Rev. 84 (2004) 1263–1314.
[9] M. Forgac, Vacuolar ATPases: rotary proton pumps in physiology and pathophysiology, Nat. Rev. Mol. Cell. Biol. 8 (2007) 917–929.
[10] G. Grüber, V. Marshansky, New insights into structure–function relationships between archeal ATP synthase (A1A0) and vacuolar type ATPase (V1V0), Bioessays 30 (2008) 1096–1109.
[11] D. Brown, S. Breton, D.A. Ausiello, V. Marshansky, Sensing, signaling and sorting events in kidney epithelial cell physiology, Traffic 10 (2009) 275–284.
[12] K.G. Blake-Palmer, F.E. Karet, Cellular physiology of the renal H+ ATPase, Curr. Opin. Nephrol. Hypertens. 18 (2009) 433–438.
[13] Y. Wang, M. Toei, M. Forgac, Analysis of the membrane topology of transmembrane segments in the C-terminal hydrophobic domain of the yeast vacuolar ATPase subunit a (Vph1p) by chemical modification, J. Biol. Chem. 283 (2008) 20696–20702.
[14] T. Toyomura, T. Oka, C. Yamaguchi, Y. Wada, M. Futai, Three subunit a isoforms of mouse vacuolar H(+)-ATPase. Preferential expression of the a3 isoform during osteoclast differentiation, J. Biol. Chem. 275 (2000) 8760–8765.
[15] T. Oka, Y. Murata, M. Namba, T. Yoshimizu, T. Toyomura, A. Yamamoto, G.H. Sun-Wada, N. Hamasaki, Y. Wada, M. Futai, a4, a unique kidney-specific isoform of mouse vacuolar H+-ATPase subunit a, J. Biol. Chem. 276 (2001) 40050–40054.
[16] A.N. Smith, J. Skaug, K.A. Choate, A. Nayir, A. Bakkaloglu, S. Ozen, S.A. Hulton, S.A. Sanjad, E.A. Al-Sabban, R.P. Lifton, S.W. Scherer, F.E. Karet, Mutations in ATP6N1B, encoding a new kidney vacuolar proton pump 116-kD subunit, cause recessive distal renal tubular acidosis with preserved hearing, Nat. Genet. 26 (2000) 71–75.
[17] A.N. Smith, K.E. Finberg, C.A. Wagner, R.P. Lifton, M.A. Devonald, Y. Su, F.E. Karet, Molecular cloning and characterization of Atp6n1b: a novel fourth murine vacuolar H+-ATPase a-subunit gene, J. Biol. Chem. 276 (2001) 42382–42388.
[18] T. Xu, E. Vasilyeva, M. Forgac, Subunit interactions in the clathrin-coated vesicle vacuolar (H(+))–ATPase complex, J. Biol. Chem. 274 (1999) 28909–28915.
[19] C. Landolt-Marticorena, K.M. Williams, J. Correa, W. Chen, M.F. Manolson, Evidence that the NH2 terminus of vph1p, an integral subunit of the V0 sector of the yeast V-ATPase, interacts directly with the Vma1p and Vma13p subunits of the V1 sector, J. Biol. Chem. 275 (2000) 15449–15457.
[20] T. Inoue, M. Forgac, Cysteine-mediated cross-linking indicates that subunit C of the V-ATPase is in close proximity to subunits E and G of the V1 domain and subunit a of the V0 domain, J. Biol. Chem. 280 (2005) 27896–27903.
[21] J. Qi, M. Forgac, Function and subunit interactions of the N-terminal domain of subunit a (Vph1p) of the yeast V-ATPase, J. Biol. Chem. 283 (2008) 19274–19282.
[22] E.E. Norgett, K.J. Borthwick, R.S. Al-Lamki, Y. Su, A.N. Smith, F.E. Karet, V1 and V0 domains of the human H+-ATPase are linked by an interaction between the G and a subunits, J. Biol. Chem. 282 (2007) 14421–14427.
[23] M. Lu, L.S. Holliday, L. Zhang, W.A. Dunn Jr., S.L. Gluck, Interaction between aldolase and vacuolar H+-ATPase: evidence for direct coupling of glycolysis to the ATP-hydrolyzing proton pump, J. Biol. Chem. 276 (2001) 30407–30413.
[24] M. Lu, Y.Y. Sautin, L.S. Holliday, S.L. Gluck, The glycolytic enzyme aldolase mediates assembly, expression, and activity of vacuolar H+-ATPase, J. Biol. Chem. 279 (2004) 8732–8739.
[25] Y.Y. Sautin, M. Lu, A. Gaugler, L. Zhang, S.L. Gluck, Phosphatidylinositol 3-kinase-mediated effects of glucose on vacuolar H+-ATPase assembly, translocation, and acidification of intracellular compartments in renal epithelial cells, Mol. Cell. Biol. 25 (2005) 575–589.
[26] M. Lu, D. Ammar, H. Ives, F. Albrecht, S.L. Gluck, Physical interaction between aldolase and vacuolar H+-ATPase is essential for the assembly and activity of the proton pump, J. Biol. Chem. 282 (2007) 24495–24503.
[27] Y. Su, A. Zhou, R.S. Al-Lamki, F.E. Karet, The a-subunit of the V-type H+-ATPase interacts with phosphofructokinase-1 in humans, J. Biol. Chem. 278 (2003) 20013–20018.
[28] Y. Su, K.G. Blake-Palmer, S. Sorrell, B. Javid, K. Bowers, A. Zhou, S.H. Chang, S. Qamar, F.E. Karet, Human H+ATPase a4 subunit mutations causing renal tubular acidosis reveal a role for interaction with phosphofructokinase-1, Am. J. Physiol. Renal Physiol. 295 (2008) F950–F958.
[29] H.R. Bourne, D.A. Sanders, F. McCormick, The GTPase superfamily: a conserved switch for diverse cell functions, Nature 348 (1990) 125–132.
[30] J.G. Donaldson, R.D. Klausner, ARF: a key regulatory switch in membrane traffic and organelle structure, Curr. Opin. Cell Biol. 6 (1994) 527–532.
[31] C. D'Souza-Schorey, P. Chavrier, ARF proteins: roles in membrane traffic and beyond, Nat. Rev. Mol. Cell. Biol. 7 (2006) 347–358.
[32] J.P. DiNitto, A. Delprato, M.T. Gabe Lee, T.C. Cronin, S. Huang, A. Guilherme, M.P. Czech, D.G. Lambright, Structural basis and mechanism of autoregulation in 3-phosphoinositide-dependent Grp1 family Arf GTPase exchange factors, Mol. Cell 28 (2007) 569–583.
[33] J.E. Casanova, Regulation of Arf activation: the Sec7 family of guanine nucleotide exchange factors, Traffic 8 (2007) 1476–1485.
[34] L.C. Santy, S.R. Frank, J.C. Hatfield, J.E. Casanova, Regulation of ARNO nucleotide exchange by a PH domain electrostatic switch, Curr. Biol. 9 (1999) 1173–1176.
[35] J.A. Marles, S. Dahesh, J. Haynes, B.J. Andrews, A.R. Davidson, Protein–protein interaction affinity plays a crucial role in controlling the Sho1p-mediated signal transduction pathway in yeast, Mol. Cell 14 (2004) 813–823.
[36] D.G. Kneller, T.D. Goddar, SPARKY 3.105, in: U.o.C.e. Edit (Ed.), 1997, San Francisco, CA.
[37] K. Wüthrich, NMR of Proteins and Nucleic acids, Wiley, Interscience, New York, 1986.
[38] T. Herrmann, P. Güntert, K. Wüthrich, Protein NMR structure determination with automated NOE assignment using the new software CANDID and the torsion angle dynamics algorithm DYANA, J. Mol. Biol. 319 (2002) 209–227.
[39] A. Lupas, M. Van Dyke, J. Stock, Predicting coiled coils from protein sequences, Science 252 (1991) 1162–1164.
[40] D.T. Jones, Protein secondary structure prediction based on position-specific scoring matrices, J. Mol. Biol. 292 (1999) 195–202.
[41] L.J. McGuffin, K. Bryson, D.T. Jones, The PSIPRED protein structure prediction server, Bioinformatics 16 (2000) 404–405.
[42] M.A. Marti-Renom, A.C. Stuart, A. Fiser, R. Sanchez, F. Melo, A. Sali, Comparative protein structure modeling of genes and genomes, Annu. Rev. Biophys. Biomol. Struct. 29 (2000) 291–325.
[43] P.R. Hiesinger, A. Fayyazuddin, S.Q. Mehta, T. Rosenmund, K.L. Schulze, R.G. Zhai, P. Verstreken, Y. Cao, Y. Zhou, J. Kunz, H.J. Bellen, The v-ATPase Vo subunit a1 is required for a late step in synaptic vesicle exocytosis in *Drosophila*, Cell 121 (2005) 607–620.
[44] P. Chardin, S. Paris, B. Antonny, S. Robineau, S. Beraud-Dufour, C.L. Jackson, M. Chabre, A human exchange factor for ARF contains Sec7- and pleckstrin-homology domains, Nature 384 (1996) 481–484.
[45] N. Guex, M.C. Peitsch, SWISS-MODEL and the Swiss-PdbViewer: an environment for comparative protein modeling, Electrophoresis 18 (1997) 2714–2723.
[46] D. Van Der Spoel, E. Lindahl, B. Hess, G. Groenhof, A.E. Mark, H.J. Berendsen, GROMACS: fast, flexible, and free, J. Comput. Chem. 26 (2005) 1701–1718.
[47] M. Mansour, S.Y. Lee, B. Pohajdak, The N-terminal coiled coil domain of the cytohesin/ARNO family of guanine nucleotide exchange factors interacts with the scaffolding protein CASP, J. Biol. Chem. 277 (2002) 32302–32309.
[48] S. Chantalat, S.K. Park, Z. Hua, K. Liu, R. Gobin, A. Peyroche, A. Rambourg, T.R. Graham, C.L. Jackson, The Arf activator Gea2p and the P-type ATPase Drs2p interact at the Golgi in *Saccharomyces cerevisiae*, J. Cell Sci. 117 (2004) 711–722.
[49] M. Yamamoto, S. Unzai, S. Saijo, K. Ito, K. Mizutani, C. Suno-Ikeda, Y. Yabuki-Miyata, T. Terada, M. Toyama, M. Shirouzu, T. Kobayashi, Y. Kakinuma, I. Yamato, S. Yokoyama, S. Iwata, T. Murata, Interaction and stoichiometry of the peripheral stalk subunits NtpE and NtpF and the N-terminal hydrophilic domain of NtpI of *Enterococcus hirae* V-ATPase, J. Biol. Chem. 283 (2008) 19422–19431.
[50] Y.R. Thaker, C. Hunke, Y.H. Yau, S.G. Shochat, Y. Li, G. Grüber, Association of the eukaryotic V1VO ATPase subunits a with d and d with A, FEBS Lett. 583 (2009) 1090–1095.
[51] J. Cherfils, J. Menetrey, M. Mathieu, G. Le Bras, S. Robineau, S. Beraud-Dufour, B. Antonny, P. Chardin, Structure of the Sec7 domain of the Arf exchange factor ARNO, Nature 392 (1998) 101–105.